

Non-thermal plasma-assisted growth of ZnWO₄ hierarchical nanostructures: morphology, structure and photoactivity

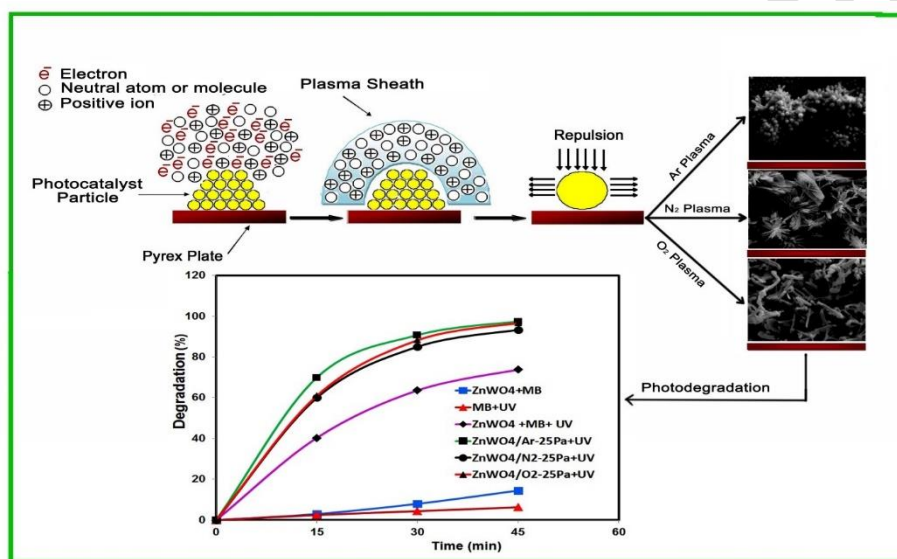
Mitra Hafezi^a, Hadi Fallah Moafi^{*a}, Mohammad Ali Zanjanchi^a, Sirous Khorram^b

^aDepartment of Chemistry, Faculty of Science, University of Guilan, P.O. Box 1914, Rasht, Iran

^bResearch Institute for Applied Physics and Astronomy, University of Tabriz, Tabriz, 51666-14766, Iran

*Corresponding author E-mail: Fallah.m@guilan.ac.ir, Phone: 981333367262

GRAPHICAL ABSTRACT



Abstract

Zinc tungstate (ZnWO₄) photocatalyst was synthesized by precipitation method and treated with different non-thermal plasma to study its morphology, structure and photocatalytic activity. The X-ray diffraction results revealed that the plasma-treated ZnWO₄ exhibited only wolframite structure and its crystallinity was preserved. The SEM images of the samples demonstrated that the morphology of ZnWO₄ was changed from non-uniform particle to flower and rod-like following plasma treatment. The enhanced photocatalytic activity of the treated ZnWO₄ sample may be associated with the enhancement in the particle size reduction and increase of the surface

area. Also, charge separation efficiency due to well-constructed space charge region along the longitudinal direction of the nano ZnWO_4 may be affected the photocatalytic activity.

Keywords: Zinc tungstate, Non-thermal Plasma, Hierarchical, Morphology, Photocatalysis.

1 Introduction

Exploring and control over the orientation and the shape of inorganic nanostructures have been an interesting long-standing goal in order to reveal the relationship between crystal structures and their properties [1]. Recently, substantial research has been conducted on the fabrication of the ZnWO_4 nanostructures, and developing attention has been devoted to the self-assembly of nano ZnWO_4 with low-dimensional and controllable shape into hierarchical structures. In comparison to mono-morphological structures, these hierarchical structures have demonstrated improved performance in functional devices such as sensors, batteries, electronics and in photocatalysis [2-8]. Among these various applications, the photocatalysis properties of ZnWO_4 nanostructure have been extensively investigated [6-8]. Over the past decade, many researches dedicated to improve the photocatalytic activity of ZnWO_4 such as crystallinity controlling [9], coupling with other semiconductors [10-12], heterojunction [13-15] modification of morphologies [16] and ion doping [7, 17,18]. For example, Gao *et al.* investigated that bismuth-

anchored ZnWO_4 shows higher photocatalytic activity than that of single ZnWO_4 due to the surface plasmon resonance (SPR) effect of Bi nanoparticles [7]. Su *et al.* prepared Sn^{2+} -doped ZnWO_4 nanocrystals with controlled particle sizes *via* a microwave-assisted hydrothermal method [17]. Their results showed that the tin-doped ZnWO_4 nanocrystals provide a significant visible light photocatalytic activity owing to the extension of its photoresponse region, improvement of the electronic structure, crystallinity and remarkable band gap narrowing. These can be attributed to the surface doping effects as well as lattice variations. Recently, for improved photoinduced charge carriers separation and reducing the recombination of electron-hole pairs, ZnWO_4 was coupled with other semiconducting materials such as, ZnO , Bi_2WO_6 , Ag/AgBr , Ag/AgCl , BiOI , In_2S_3 , Ag_3PO_4 , Fe_2O_3 , CdWO_4 etc. to fabricate various heterostructures [10-12, 19-25]. For instance, Wang *et al.* have reported $\text{In}_2\text{S}_3/\text{ZnWO}_4$ composites, which are exhibited enhanced photo-catalytic activity than that of the individual In_2S_3 and ZnWO_4 [22]. Guo *et al.* investigated that $\text{ZnWO}_4/\text{Ag}_3\text{PO}_4$ composite exhibited a higher hydrogen production rate than that of the single Ag_3PO_4 substrate [23]. They found that the photoluminescence measurement shows a more efficient photoinduced charge separation and transfer in $\text{ZnWO}_4/\text{Ag}_3\text{PO}_4$ composite. Many methods such as hydrothermal method [2-5, 8] and ultrasonic spray pyrolysis [6,7] have been developed to produce ZnWO_4 hierarchical nanostructures. Among the procedures used for the synthesis of ZnWO_4 hierarchical, hydrothermal method is widely used. The hydrothermal method has become the subject of interest in the synthesis of hierarchical nanostructures because of its simple procedure, moderate-temperature, and low cost.

Newly, plasma technology has been employed for surface modification, morphological change, and improvement of the activity and stability of catalysts [26-33]. However, there are limited

studied on the morphological changes created by the plasma treatments. This protocol will improve the catalytic activity of certain materials. For example, Khataee *et al.* [26] have modified the clinoptilolite microparticles to nanorod structures by non-thermal plasma. Also, Zen-Hung *et al.* have investigated the conversion of Ag colloids to flower-like Ag₂O nanostructures by O₂ and H₂ plasma treatment which was used for degradation methylene blue [27]. Moafi *et al.* [32] investigated the effects of non-thermal plasma on the morphology of Ce-ZnO nanocomposite. It was observed that the photocatalytic activity of plasma treated samples is higher than that of the untreated Ce-ZnO. In this work, a facile, novel, one-step and environmentally-friendly strategy for the preparation of hierarchical ZnWO₄ is presented. This would be performed *via* argon, nitrogen and oxygen plasma processing. At first, ZnWO₄ nanoparticles were synthesized by the precipitation method. The obtained nanoparticles were subjected to non-thermal plasma treatment to achieve the hierarchical ZnWO₄ structures. The photocatalytic performance of ZnWO₄ hierarchical nanostructures is studied and compared with that of the untreated ZnWO₄ nanostructures. The hierarchical ZnWO₄ exhibited higher photocatalytic activities than that of the untreated ZnWO₄ sample.

2 Experimental

2.1 Chemicals and Materials

All commercial reagents such as zinc acetate dihydrate [Zn(OAc)₂·2H₂O], sodium tungstate (Na₂WO₄·2H₂O), methylene blue and sodium hydroxide were analytic grade reagents, purchased from Merck (Germany) and used without further purification. De-ionized water was used for synthesis of ZnWO₄ sample.

2.2 Synthesis of the ZnWO₄ nanoparticles

ZnWO₄ nanoparticles were synthesized by the precipitation reaction of Zn(OAc)₂·2H₂O and Na₂WO₄·2H₂O at room temperature. In a typical procedure route, Zn(OAc)₂·2H₂O (0.02 mol) was dissolved in 100 ml of de-ionized water under vigorous stirring at room temperature. Then, an aqueous solution of Na₂WO₄·2H₂O (0.02 mol) was slowly added into the solution under vigorous stirring. The solution pH was adjusted to 8 by adding NaOH solution. The white precipitate is formed. The products were filtered off and washed several times with de-ionized water and dried at 100 °C for 2h. Finally, the solid is calcined for at 500 °C for 3h.

2.3. Plasma Treatment Procedure

The description of plasma treatment procedure has been demonstrated in our previous investigation [32]. The glow discharge plasma was used for plasma-surface modification of samples as shown in Fig. 1a. The plasma reactor consists of a pyrex tube with the size of 400mm × 50mm (diameter of 50mm and length of 400mm). For plasma treatment, ZnWO₄ powder sample (1 g) was placed homogeneously on the pyrex plate and located in the positive column region of the tube. Then, different gas plasma, such as argon, nitrogen and oxygen were separately consumed as the plasma-forming gas. They were introduced into the reactor while the gas pressure was kept in the range of 15–50Pa. The plasma-treated ZnWO₄ were designated as ZnWO₄-Ar, ZnWO₄-N₂, and ZnWO₄-O₂ according to the used plasma. The photocatalytic activity of these modified samples was measured by evaluating the photodegradation of MB.

2.4 Characterization techniques

Structural identification of zinc tungstate was carried out by means of X-ray diffraction method using a D8 Bruker X-ray diffractometer with CuKα radiation. The SEM observation was performed by scanning electron microscopy (SEM, Philips XL30) attached with an energy dispersive spectroscopy (EDS) accessory for compositional analysis. The optical properties of

the samples at 200-800 nm were recorded using a UV-2100 Shimadzu spectrophotometer in the reflectance mode. A Sibata SA-1100 surface area analyzer was used for determination of BET surface area of the samples. Photoluminescence spectra (PL) of the untreated and plasma treated samples were recorded by a Hitachi F-7000 fluorescence spectrophotometer. For PL measurement, all the samples were excited at 300 nm wavelength using a xenon lamp at room temperature. The change of dye concentration was measured by a Perkin Elmer ultraviolet-visible spectrophotometer.

2.5 Photocatalytic test

The photocatalytic activity of the untreated and treated ZnWO_4 was evaluated by studying of the photodegradation of MB under UV and visible light irradiations. The photocatalytic experiment procedure has been stated in our previous study with a little change [32]. The UV irradiation was done using a krypton lamp (400 W high-pressure lamp) with maximum emission at 365 nm without filter. The visible irradiation was carried out using a tungsten lamp (200 W) without filter. They were placed vertically along at a distance of 40 cm from the sample in the reactor. The temperature of the photodegradation reaction was preserved at 25 °C using a water bath. Before illumination, the MB solution (50 ml, 1×10^{-5} M) with the appropriate amount of the catalysts (40 mg) was stirred for 20 min in dark to ensure the establishment of an adsorption-desorption equilibrium between the photocatalyst powder and MB. After that, photocatalyst powder was separated from the suspension by the centrifugal machine and the concentration of MB was analyzed with UV-Vis spectrophotometer. The change in absorbance of MB was measured at $\lambda_{\text{max}} = 665$ nm as a function of irradiation time. The concentration of MB was calculated from a standard calibration curve.

3. Results and Discussion

3.1 XRD analysis

The powder XRD patterns were used for structural identification of the untreated and plasma-treated ZnWO_4 . Fig. 2 shows the XRD patterns of the pure and plasma-treated ZnWO_4 . All the reflections can be indexed as pure monoclinic sanmartinite phase of ZnWO_4 with wolframite structure [8] in accordance with the standard data (JCPDS card 073–0554). It can be clearly seen that all the samples show high crystallinity without any impurity phases suggesting that there is no change in the crystal structure upon plasma treatment. Although, morphological observations indicate that the morphology of as-prepared ZnWO_4 changed to hierarchical flower-like or rod-like ZnWO_4 nanostructures following the plasma treatment (Fig. 3). The average grain size is calculated using the Scherrer's equation based on the FWHM of the (111) peak of the compounds. The results are summarized in Table 1. Moreover, it can be seen in Fig. 2b-2d that the broadening of the reflections associated with the ZnWO_4 phase suggests that the size of the particles is quite small. In the case of $\text{ZnWO}_4\text{-N}_2$, it was observed that the FWHM peak is broader than that of the other samples (Table 1).

3.2 Morphological and compositional analysis

The size and shape of ZnWO_4 and plasma-treated ZnWO_4 were investigated by SEM. Fig. 3 shows SEM micrographs of ZnWO_4 and plasma-treated ZnWO_4 . In Fig. 3a, the SEM micrograph of ZnWO_4 nanoparticles is illustrated. The image reveals that the most of them are irregularly shaped and approximately spherical with dimensions that are larger and smaller than 100 nm. Fig. 3b displays the SEM image of ZnWO_4 treated by argon plasma ($\text{ZnWO}_4\text{-Ar}$), indicating that the sample consists of fine particles and flower-like nanostructures. The SEM image indicates that flower like parts of the $\text{ZnWO}_4\text{-Ar}$ consists of nanorods with a diameter of less than 100 nm

which are assembled to create a three-dimensional flower-like hierarchical structure. The micrograph of the sample treated in nitrogen plasma ($\text{ZnWO}_4\text{-N}_2$) is shown in Fig. 3c. In this figure, highly uniform and sheet-shaped nanocrystals which are distributed spatially in a regular direction can be observed. It can be seen that the $\text{ZnWO}_4\text{-N}_2$ are composed by numerous ultra-thin nanosheets array with the thickness of about 10 nm which are assembled to create a three-dimensional hierarchical structure of ZnWO_4 . SEM image confirms the morphology of ZnWO_4 nanoparticles converted to the petal-like hierarchical structure after nitrogen plasma treatment. SEM image of oxygen plasma-treated sample ($\text{ZnWO}_4\text{-O}_2$) in Fig. 3d indicate that the $\text{ZnWO}_4\text{-O}_2$ consist of nanorods with dimensions that are smaller than 100 nm. This image also confirms that the morphology of initial ZnWO_4 nanoparticles is completely converted to nanorods shape after plasma treatment.

It should be noted that the plasma effect on the morphology and structure catalyst is a challenge, and further experimental exploration should be performed to predict the exact mechanism of plasma effect. Fig. 1b shows the schematic representation of plasma treatment on ZnWO_4 particles. It is recognized that the plasma consists of energetic electrons and high reactive species [26]. When the ZnWO_4 catalyst is exposed to non-thermal plasma, the particles of the catalyst perform as electron sinks [26]. Also, positive ions and neutral atom or molecules create to a plasma sheath around the catalyst. In the presence of catalyst powders density of electrons in plasma was considerably decreased which lead to the trapping of electrons [31, 33]. The electrons flow in the plasma treatment perform a strong repulsive force, which at the same time, strong coulomb repulsions exist between the electrons trapped on the same particle [26]. According to the above explanation, it is supposed that strong repulsive forces created inside and outside the structure of the ZnWO_4 nanoparticles. These powerful forces caused the bonds between the main

elements of ZnWO_4 elongated or deformed. Finally, under this condition, the deformed bonds are easily split, resulting in a severe change in the morphological and structural transformations. The chemical composition of ZnWO_4 was determined by EDX analysis. The elemental analysis by EDX is shown in Fig. 3e. The EDX spectrum of the sample clearly reveals the presence of Zn, W, O elements. Moreover, EDX results confirmed the purity of our sample detecting only Zn, W and O. The surface area of the untreated and treated ZnWO_4 samples was determined using the nitrogen gas adsorption method (Table 1). The results indicate that surface area was increased upon plasma treatment. The order of surface area was as follows: $\text{ZnWO}_4\text{-Ar} > \text{ZnWO}_4\text{-N}_2 > \text{ZnWO}_4\text{-O}_2 > \text{ZnWO}_4$.

3.3. FT -IR Study

FT-IR spectra of ZnWO_4 and plasma-treated samples are shown in Fig. 4. Several peaks identified in the range of $450\text{--}1000\text{ cm}^{-1}$ correspond to the absorption bands existing in ZnWO_4 structure (Fig. 4a). The peaks observed at 476 cm^{-1} , 545 cm^{-1} , 669 cm^{-1} , and 730 cm^{-1} , related to bending and stretching of Zn–O and W–O bands, respectively [34]. Furthermore, the peaks located at 844 cm^{-1} and 887 cm^{-1} are ascribed to the bending and stretching of vibration bands in Zn–W–O [35]. Furthermore, there were two peaks at 1654 cm^{-1} and 3460 cm^{-1} which can be attributed to the OH bending vibration band (physically adsorbed water) and stretching vibration band of O–H, respectively [36]. Infrared spectra of the treated sample by argon, nitrogen, and oxygen also showed the absorption bands existing in ZnWO_4 structure (Figs. 4a and 4b). The spectra of the treated samples were entirely unchanged.

3.4 Effects of nanostructure on the optical properties

The influences of morphology on the optical properties of ZnWO_4 photocatalysts was investigated by the UV-vis diffuse reflectance spectroscopy. The spectra of ZnWO_4 and plasma-

treated ZnWO₄ are shown in Fig. 4c. The ZnWO₄ shows no absorption in the visible region. It shows optical absorption in the UV region. The absorption of UV light by ZnWO₄ is assigned to the band transition from the occupied O 2p orbital to the empty W 5d orbital [37, 18]. In the DR spectra of ZnWO₄, peaks appeared in the range of 250 -350 nm could be attributed to direct excitation in ZnWO₄ [16]. In the treated sample, plasma treatment leads to blue-shift in the absorption edge and the decreased absorption intensity of the samples. The band gap energy (E_g) of ZnWO₄ and plasma-treated ZnWO₄ can be calculated by the equation, $E_g = 1239.8/\lambda$, where λ is the wavelength (nm) of the exciting light (Table 1). It can be stated that the difference in absorption edge for the samples obviously designates difference in the band gap of the samples. The absorption edge of the untreated ZnWO₄ sample is about 410 nm, corresponding to band gap energy of 3.02 eV. The band gap energy of the plasma-treated sample, namely, ZnWO₄-Ar, ZnWO₄-N₂, ZnWO₄-O₂ was calculated as 3.06, 3.10 and 3.14 eV, respectively. Increasing the band gap of the plasma-treated samples can be attributed to the reduction in particle size and the quantum size effect.

3.5 Photoluminescence measurements

Room temperature PL spectra of untreated and plasma-treated ZnWO₄ are shown in Fig. 5a. Fig. 5a displays PL spectra in the wavelengths ranges from the ultraviolet to the visible region (350-600 nm) for each of the samples. For oxide semiconductor material, the photoluminescence spectrum is closely related to the transfer behavior of the photogenerated electrons and holes so that it can show the recombination and separation of photoinduced charge carriers [19]. The lower PL intensity often implies the lower recombination rate of excited electrons/holes and the higher photocatalytic activity of semiconductor materials [19]. It can be clearly seen that untreated and plasma treated ZnWO₄ samples display the main emissions band at about 450-480

nm ascribed to band gap transition of ZnWO_4 [38]. The treatment of plasma weakens the PL intensity of ZnWO_4 nanoparticles. These results suggest that the recombination of the electron–hole in treated ZnWO_4 is less than that in untreated ZnWO_4 . Thus, plasma-treated photocatalyst shows higher photocatalytic activity for MB photodegradation compared to that of bare ZnWO_4 .

3.6 Evaluation of Photocatalytic Activity

3.6.1 Photodegradation of MB under UV light irradiation

The photocatalytic activity of ZnWO_4 and plasma-treated ZnWO_4 was evaluated by the degradation of MB under UV light irradiation. The results are displayed in Fig. 5b. As shown in Fig. 5b, the MB was not changed under direct photolysis (in the absence of ZnWO_4). In the presence of ZnWO_4 and absence of UV light again the MB was stable. It was observed that the direct photolysis and adsorption on ZnWO_4 were negligible as there was no obvious MB elimination in the absence of photocatalyst. In the presence of ZnWO_4 and UV light, the elimination of MB aqueous solution (50 ml, 1×10^{-5} M) was also tested. It was observed that MB was degraded under UV light irradiation (about 78% within 45 min) as shown in Fig. 5b. To evaluate the effect of plasma treatment on photoactivity of ZnWO_4 , photodegradation of $\text{ZnWO}_4\text{-Ar}$, $\text{ZnWO}_4\text{-N}_2$, and $\text{ZnWO}_4\text{-O}_2$ were also tested (under plasma gas pressure of 25 Pa for 30 min). It is seen from Fig. 5b that, the photocatalytic activity of the plasma-treated ZnWO_4 is higher than that of the untreated ZnWO_4 . About 97.4, 93.3 and 96.6% of MB were degraded using $\text{ZnWO}_4\text{/Ar}$, $\text{ZnWO}_4\text{/N}_2$, and $\text{ZnWO}_4\text{/O}_2$, respectively (45 min irradiation).

It is generally accepted that photocatalytic activity of semiconductor photocatalysts depends on the various properties such as crystallinity, size, morphology etc. These structural and physical properties are related to each other and can be finally ascribed to the photo-induced charge

properties of photocatalysts [39]. Although the crystallinity of untreated and treated ZnWO₄ photocatalysts with different plasma was similar, their photocatalytic activities were different, indicating that the morphology of ZnWO₄ affects a great consequence on photocatalytic activity. In plasma treated ZnWO₄ samples with the hierarchical structure (such as nanorods), despite the influence of factors such as large BET surface area and smaller particle size, the largest number of surface states may promote the separation of the electron-hole pairs and enhance its photocatalytic activity, as suggested by He et.al [39]. It is well known that, for semiconductor photocatalysis, the effective separation of photogenerated electron-hole pairs after light irradiation is the significant process. The electron and hole pairs on the semiconductor surfaces captured by O₂ and H₂O molecules adsorbed on the surface to produce •O₂⁻ and •OH radicals, which can lead to the efficient destruction of air pollutants. During the photocatalysis processes, the formation of •OH and •O₂⁻ radicals play a crucial role in the photodecomposition of pollutants. The formation of •OH and •O₂⁻ radicals during the photocatalysis processes confirms by ESR spectra. Yu *et. al*[6] reported both •OH and •O₂⁻ radicals were involved in the photocatalytic reaction associated with ZnWO₄ samples. Meanwhile, the improved photocatalytic efficiency of ZnWO₄ hierarchical structure could be attributed to aspect ratio and the space charge region. Di *et al* [8] reported that the space charge region well developed along the longitudinal direction of ZnWO₄ nanorods, which caused an effective reduction in the chance of e/h⁺ recombination. Consequently, the recombination of photogenerated electron-hole pairs decreased with increasing aspect ratio [8].

3.6.2 Influence of plasma gas pressure on photodegradation

Effects of plasma gas pressure on the photocatalytic degradation of MB are shown in Fig. 6. For this purpose, ZnWO₄ samples were treated at 15, 25 and 50 Pa for 30 min. It was observed that

with increasing of plasma gas pressure photodegradation of MB was improved. As shown in Fig. 6, the MB degradation by the ZnWO_4 treated at the plasma gas pressure of 25 Pa is higher than that at 15 Pa. Comparison of photoactivity of samples treated at 25 and 50 Pa revealed that the photocatalytic efficiency of the samples at 50 Pa is almost the same as that at 25 Pa. It can be believed from these results that the influence of gas pressure on the efficiency of photocatalytic activity is effective up to 25 Pa. Thus, 25 Pa of plasma gas pressure is considered for the optimal experimental condition.

3.6.3 Effect of catalyst dosage and solution pH

Photocatalytic activity of semiconductor-based materials strongly depends on catalyst dosage and solution pH. The effect of loading of plasma-treated ZnWO_4 samples on the degradation of MB was evaluated in the range of 40–80 mg at initial pH 7 and dye concentration of 1×10^{-5} M. As illustrated in Fig. 7, the degradation reaction of MB enhances with increasing of catalyst dosage from 40 to 80 mg at 30 min irradiation time. When catalyst concentration increased from 40 to 80 mg, the photodegradation of MB increased in all samples. It is clear that from Fig. 7, the MB degradation using 60 mg plasma-treated ZnWO_4 catalyst is higher than that of catalyst weighted 40 mg. Meanwhile, the photoactivity of the catalyst samples at 80 mg dosage is approximately same to 60 mg. It can be concluded that a catalyst weight of 60 mg is adequate. As a result, the amount of 60 mg of catalyst as the suitable amount is appropriated for the optimal experimental conditions. Similar works were reported in other studies on photodegradation of various pollutants [19, 40]. With increasing of weight, the percentage of degradation should be increased, due to the increased number of available adsorption and catalytic active sites on the photocatalyst [40]. However, when catalyst dosage is increased, light scattering and screening effect of catalyst reducing its specific activity. Also, the agglomeration

of photocatalyst decreasing the surface available for photon absorption and dye adsorption, resulting in the decreasing of the percent of degradation [19].

The effect of solution pH on the photocatalytic activity of ZnWO_4 was checked out by keeping other experimental conditions (catalyst dosage of 60 mg and the dye concentration of 1×10^{-5} M) in the constant values of 3 (not shown in Fig. 8), 7 and 10. It is evident that MB degradation was strongly dependent on pH parameter. It was found that in acidic pH (pH=3) under the dark condition at 20 min (in the absence of light illumination) over 90% of MB was adsorbed on the surface of ZnWO_4 and treated ZnWO_4 even at different dye concentration (Table 1). For this reason, pH 7 results were compared with pH 10 results in Fig. 8. When the initial pH of dye solutions was increased to 7 and 10, the degradation efficiency of MB reached to the highest value during the 30 min reaction. It is clear that from Fig. 8, the photocatalytic activity of the samples at pH 10 is almost the same as that at pH 7. It can be thought from these results that the effect of solution pH on the photocatalytic activity might reach the upper limit at pH 7. Therefore, pH 7 is adopted for the optimum experimental condition.

3.6.4 Stability of plasma treated ZnWO_4

Stability and durability of the photocatalysts is an important parameter for practical applications. In order to explore reusability of the plasma-treated ZnWO_4 , the degradation experiments were tested in optimum conditions. Fig. 9 shows the six-time repeatability experiments of photodegradation of MB under UV light irradiation. Under UV illumination, the repeatability experiments were performed in two different concentrations of dye, that is, at concentrations of 2×10^{-5} and 3×10^{-5} M (Fig. 9a and 9b). After each degradation experiment, the used treated ZnWO_4 samples were recycled by filtration, washed with de-ionized water, and dried at 60°C for 12 h and used again for the next run. Although the degradation efficiency of the plasma-

treated ZnWO₄ nanostructures decreased slightly after each run, the catalyst still exhibited significant activity during the six cycles of degradation tests (Fig. 9).

3.6.5 Photodegradation of MB under visible light irradiation

Photocatalytic activity of ZnWO₄ and plasma-treated ZnWO₄ hierarchical nanostructures was evaluated under visible light illumination as well. The results are shown in Fig. 9c. In the presence of ZnWO₄ and visible light degradation of MB (50 ml, 1×10^{-5} M) was tested. It was observed that about 60% of MB was degraded within 90 min. To evaluate the effect of plasma treatment on photoactivity of the ZnWO₄, photodegradation experiments on MB were carried out by ZnWO₄ samples modified by argon, nitrogen, and oxygen. The condition of plasma treatment was similar to those obtained for UV status (catalyst weights = 60 mg, pH = 7, dye concentration = 1×10^{-5} M, plasma gas pressure = 25Pa and temperature = 25 °C). It is seen from Fig. 9c that, the photocatalytic activity of the plasma-treated ZnWO₄ samples are higher than that of ZnWO₄. The degradation efficiency for MB solution within 90 min illumination was about 90.1, 79.6 and 84.3% for ZnWO₄-Ar, ZnWO₄-N₂ and ZnWO₄-O₂, respectively.

Fig. 9d shows the six-time repeatability experiments of photodegradation of MB under visible light irradiation. Degradation efficiency of the plasma-treated ZnWO₄ nanostructures was decreased after run 5 and 6, but the catalyst still exhibited photoactivity throughout the six cycles of degradation tests. The results demonstrated that the plasma-treated ZnWO₄ hierarchical nanostructure was practically stable to UV and visible light and the conditions used and can be used as photocatalyst for decontamination.

4 Conclusion

In the present work, the effect of non-thermal plasma is studied on the morphology, structure and photocatalytic activity of ZnWO_4 . The ZnWO_4 nanoparticles were prepared by precipitation method and modified by different non-thermal plasma. XRD results confirmed that the crystal structure of the samples was not changed after treatment using the different non-thermal plasma. SEM images of the treated ZnWO_4 showed that the morphology of the samples was entirely changed to flower like and fine nanoparticle by argon plasma. They were converted to nanorod-like morphology using nitrogen and oxygen plasma treatments. The photocatalytic efficiency of the untreated and plasma-treated samples demonstrated that the dye degradation efficiency was improved. In order to achieve the optimum condition for maximum efficiency, the effect of plasma gas pressure, catalyst dosage and pH was investigated on the degradation of MB. The plasma-treated ZnWO_4 nanostructures exhibited much higher photocatalytic activities than that of the pristine ZnWO_4 . The reusability of the plasma-treated samples was also tested under visible-light and UV-light irradiation.

Acknowledgments

The authors thank the University of Guilan, Iran for providing financial assistance for this research project.

References:

1. Wang J, Hou S, Zhang L, et al (2014) Ultra-rapid formation of ZnO hierarchical structures from dilution-induced supersaturated solutions. *CrystEngComm* **16**:7115–7123
2. Cao X, Wu W, Chen N, et al (2009) An ether sensor utilizing cataluminescence on nanosized ZnWO_4 . *Sens. Actuators B*. 137:83–87
3. Li C, Liang Y, Mao J, et al (2016) Enhancement of gas-sensing abilities in p-type ZnWO_4 by local modification of Pt nanoparticles. *Anal. Chim. Acta*. 927:107–116

4. Shi N, Xiong S, Wu F, et al (2017) Hydrothermal Synthesis of ZnWO_4 Hierarchical Hexangular Microstars for Enhanced Lithium-Storage Properties. *Eur. J. Inorg. Chem.* 2017:734–740
5. Guan B, Hu L, Zhang G, et al (2014) Facile synthesis of ZnWO_4 nanowall arrays on Ni foam for high performance supercapacitors. *RSC Adv* 4:4212–4217
6. Huang Y, Gao Y, Zhang Q, et al (2016) Hierarchical porous ZnWO_4 microspheres synthesized by ultrasonic spray pyrolysis: Characterization, mechanistic and photocatalytic NO x removal studies. *Appl. Catal. A: Gen.* 515:170–178
7. Gao Y, Huang Y, Li Y, et al (2016) Plasmonic Bi/ZnWO_4 Microspheres with Improved Photocatalytic Activity on NO Removal under Visible Light. *ACS Sustainable Chem. Eng.* 4:6912–6920
8. Li D, Shi R, Pan C, et al (2011) Influence of ZnWO_4 nanorod aspect ratio on the photocatalytic activity. *CrystEngComm* 13:4695
9. Liu B, Yu S-H, Li L, et al (2004) Nanorod-Direct Oriented Attachment Growth and Promoted Crystallization Processes Evidenced in Case of ZnWO_4 . *J. Phys. Chem.B.* 108:2788–2792
10. Leonard KC, Nam KM, Lee HC, et al (2013) $\text{ZnWO}_4/\text{WO}_3$ Composite for Improving Photoelectrochemical Water Oxidation. *J. Phys. Chem. C.* 117:15901–15910
11. Hamrouni A, Moussa N, Di Paola A, et al (2014) Characterization and photoactivity of coupled $\text{ZnO}-\text{ZnWO}_4$ catalysts prepared by a sol–gel method. *Appl. Catal. B: Environ.* 154–155:379–385
12. He D, Wang L, Xu D, et al (2011) Investigation of Photocatalytic Activities over $\text{Bi}_2\text{WO}_6/\text{ZnWO}_4$ Composite under UV Light and Its Photoinduced Charge Transfer Properties. *ACS Appl. Mater. Interfaces.* 3:3167–3171
13. Wang F, Li W, Gu S, et al (2016) Fabrication of $\text{FeWO}_4@\text{ZnWO}_4/\text{ZnO}$ Heterojunction Photocatalyst: Synergistic Effect of ZnWO_4/ZnO and $\text{FeWO}_4@\text{ZnWO}_4/\text{ZnO}$ Heterojunction Structure on the Enhancement of Visible-Light Photocatalytic Activity. *ACS Sustainable Chem. Eng.* 4:6288–6298
14. Sun L, Zhao X, Jia C-J, et al (2012) Enhanced visible-light photocatalytic activity of $\text{g-C}_3\text{N}_4-\text{ZnWO}_4$ by fabricating a heterojunction: investigation based on experimental and theoretical studies. *J. Mater. Chem.* 22:23428
15. Wang Y, Wang Z, Muhammad S, He J (2012) Graphite-like C_3N_4 hybridized ZnWO_4 nanorods: Synthesis and its enhanced photocatalysis in visible light. *CrystEngComm* 14:5065
16. Lin J, Lin J, Zhu Y (2007) Controlled Synthesis of the ZnWO_4 Nanostructure and Effects on the Photocatalytic Performance. *Inorg. Chem.* 46:8372–8378

17. Su Y, Zhu B, Guan K, et al (2012) Particle Size and Structural Control of ZnWO₄ Nanocrystals via Sn²⁺ Doping for Tunable Optical and Visible Photocatalytic Properties. *J. Phys. Chem. C*. 116:18508–18517
18. Huang G, Zhu Y (2007) Enhanced Photocatalytic Activity of ZnWO₄ Catalyst via Fluorine Doping. *J. Phys. Chem. C*. 111:11952–11958
19. Li K, Xue J, Zhang Y, et al (2014) ZnWO₄ nanorods decorated with Ag/AgBr nanoparticles as highly efficient visible-light-responsive photocatalyst for dye AR18 photodegradation. *Appl. Surf. Sci.* 320:1–9
20. Ke J, Niu C, Zhang J, Zeng G (2014) Significantly enhanced visible light photocatalytic activity and surface plasmon resonance mechanism of Ag/AgCl/ZnWO₄ composite. *J. Mol. Catal. A: Chem.* 395:276–282
21. Li P, Zhao X, Jia C, et al (2013) ZnWO₄/BiOI heterostructures with highly efficient visible light photocatalytic activity: the case of interface lattice and energy level match. *J. Mater. Chem. A*. 1:3421
22. Wang F, Li W, Gu S, et al (2015) Novel In₂S₃/ZnWO₄ heterojunction photocatalysts: facile synthesis and high-efficiency visible-light-driven photocatalytic activity. *RSC Adv.* 5:89940–89950
23. Guo R, Wu J, Xu A, et al (2016) ZnWO₄/Ag₃PO₄ composites with an enhanced photocatalytic activity and stability under visible light. *RSC Adv.* 6:114818–114824
24. Sadiq MMJ, Shenoy US, Bhat DK (2016) Novel RGO–ZnWO₄–Fe₃O₄ nanocomposite as high performance visible light photocatalyst. *RSC Adv.* 6:61821–61829
25. Li D, Xue J, Bai X (2016) Synthesis of ZnWO₄/CdWO₄ core–shell structured nanorods formed by an oriented attachment mechanism with enhanced photocatalytic performances. *CrystEngComm* 18:309–315
26. Khataee A, Bozorg S, Khorram S, et al (2013) Conversion of Natural Clinoptilolite Microparticles to Nanorods by Glow Discharge Plasma: A Novel Fe-Impregnated Nanocatalyst for the Heterogeneous Fenton Process. *Ind. Eng. Chem. Res.* 52:18225–18233
27. Yang Z-H, Ho C-H, Lee S (2015) Plasma-induced formation of flower-like Ag₂O nanostructures. *Appl. Surf. Sci.* 349:609–614
28. Rahemi N, Haghighi M, Babaluo AA, et al (2013) Non-thermal plasma assisted synthesis and physicochemical characterizations of Co and Cu doped Ni/Al₂O₃ nanocatalysts used for dry reforming of methane. *Int. J. Hydrogen Energy*. 38:16048–16061
29. He D, Sun Y, Xin L, Feng J (2014) Aqueous tetracycline degradation by non-thermal plasma combined with nano-TiO₂. *Chem. Eng. J.* 258:18–25

30. Zhu B, Jang BW-L (2014) Insights into surface properties of non-thermal RF plasmas treated Pd/TiO₂ in acetylene hydrogenation. *J. Mol. Catal. A: Chem.* 395:137–144
31. Liu C, Zou J, Yu K, et al (2006) Plasma application for more environmentally friendly catalyst preparation. *Pure Appl. Chem.* 78:1227–1238
32. Moafi HF, Hafezi M, Khorram S, Zanjanchi MA (2017) The Effects of Non-thermal Plasma on the Morphology of Ce-doped ZnO: Synthesis, Characterization and Photocatalytic Activity of Hierarchical Nanostructures. *Plasma Chem Plasma Process.* 37:159–176
33. Liu C, Vissokov GP, Jang BW-L (2002) Catalyst preparation using plasma technologies. *Catal Today* 72:173–184
34. Huang G, Zhu Y (2007) Synthesis and photocatalytic performance of ZnWO₄ catalyst. *Mater. Sci. Eng. B.* 139:201–208
35. Mancheva M, Iordanova R, Dimitriev Y (2011) Mechanochemical synthesis of nanocrystalline ZnWO₄ at room temperature. *J. Alloy Compd.* 509:15–20
36. Amouzegar Z, Naghizadeh R, Rezaie HR, et al (2015) Cubic ZnWO₄ nano-photocatalysts synthesized by the microwave-assisted precipitation technique. *Ceram. Int.* 41:1743–1747
37. Fu H, Lin J, Zhang L, Zhu Y (2006) Photocatalytic activities of a novel ZnWO₄ catalyst prepared by a hydrothermal process. *Appl. Catal. A: Gen.* 306:58–67
38. Bonanni M, Spanhel L, Lerch M, et al (1998) Conversion of Colloidal ZnO–WO₃ Heteroaggregates into Strongly Blue Luminescing ZnWO₄ Xerogels and Films. *Chem Mater* 10:304–310
39. He D, Zhang X, Xie T, et al (2011) Studies of photo-induced charge transfer properties of ZnWO₄ photocatalyst. *Appl. Surf. Sci.* 257:2327–2331
40. Konstantinou IK, Albanis TA (2004) TiO₂-assisted photocatalytic degradation of azo dyes in aqueous solution: kinetic and mechanistic investigations: A review. *Appl. Catal. B: Environ.* 49:1–14

Table 1: Some characteristics of ZnWO₄ and plasma-treated ZnWO₄

Samples	Crystalline structure	Absorption edge (nm)	Band gap energy (eV)	BET surface area (m ² /g)	XRD crystal size (nm)	FWHM of XRD analysis	SEM crystal size (nm)
ZnWO ₄	Monoclinic	410	3.02	41.10	16.55	0.4920	~100

ZnWO ₄ -Ar	Monoclinic	405	3.06	78.23	16.55	0.4920	<50
ZnWO ₄ -N ₂	Monoclinic	400	3.10	61.32	13.79	0.5904	<50
ZnWO ₄ -O ₂	Monoclinic	395	3.14	59.65	16.55	0.4920	<50

*Adsorption results of samples at pH 3 in various dye concentration

Sample	Adsorption (1×10 ⁻⁵ M)	Adsorption (2×10 ⁻⁵ M)	Adsorption (3×10 ⁻⁵ M)
ZnWO ₄	94.5%	93.2%	92.5%
ZnWO ₄ /Ar	97.1%	95.3%	94.2%
ZnWO ₄ /O ₂	97.4%	95.0%	93.1%
ZnWO ₄ /N ₂	96.6%	94.1%	95.0%

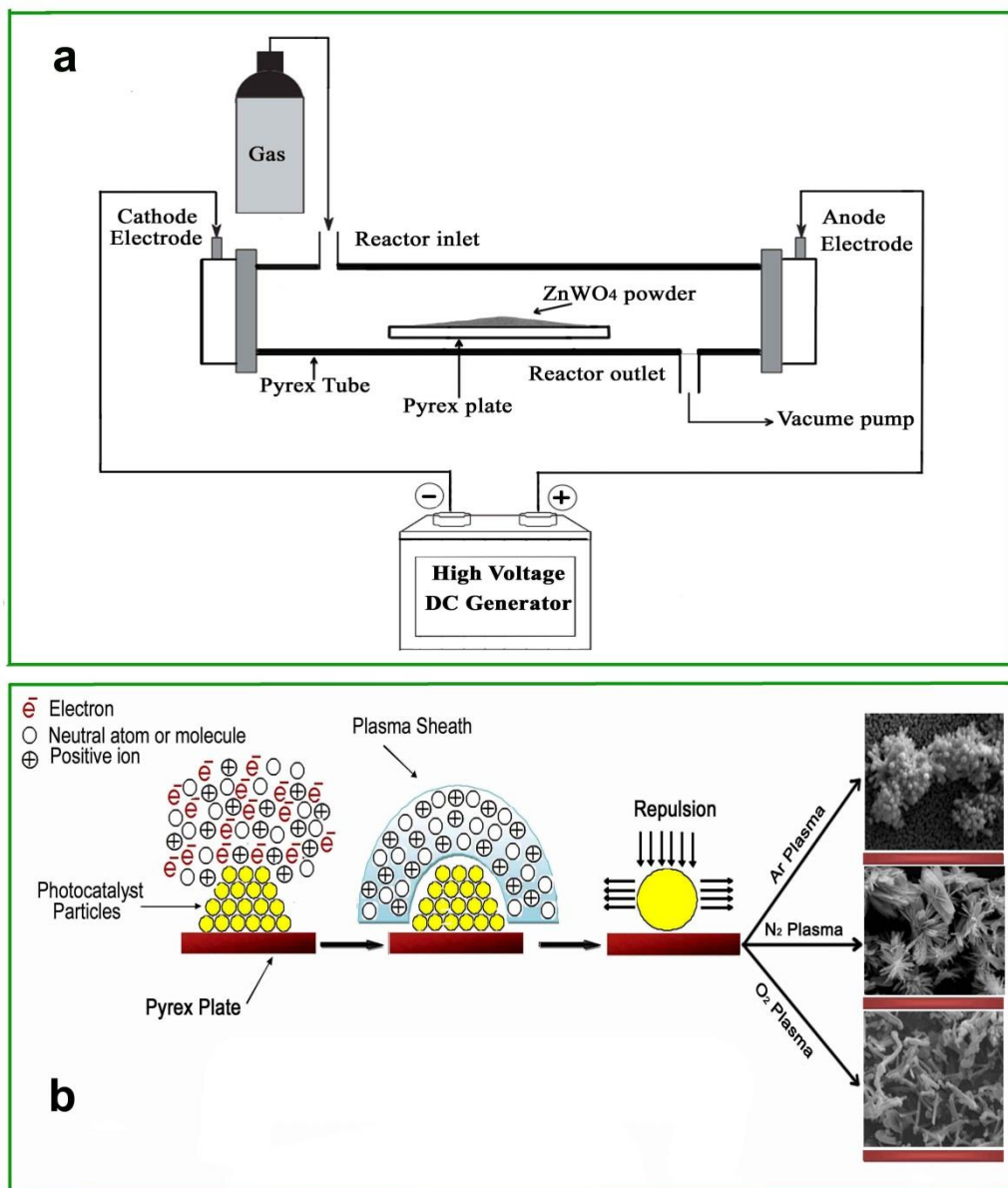


Fig. 1. (a): Schematic diagram of the glow discharge plasma system for treatment of synthesized ZnWO₄, **(b)** Schematic representation of plasma-treatment on the ZnWO₄.

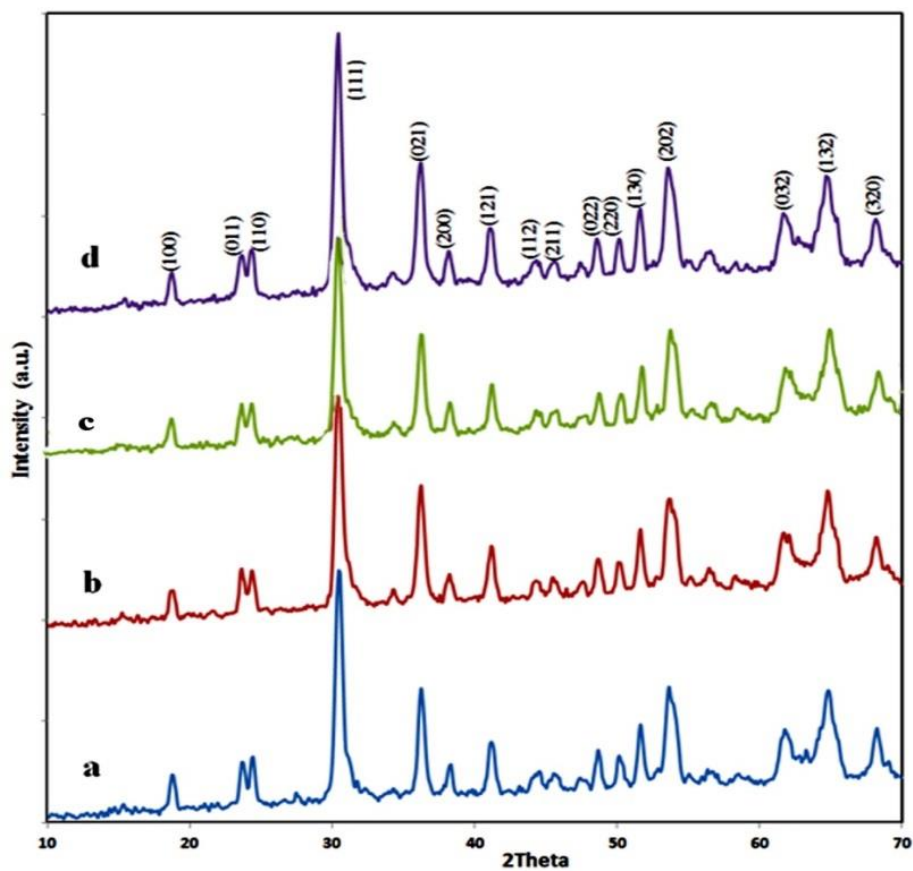


Fig. 2. XRD pattern of untreated ZnWO₄ and plasma treated ZnWO₄: (a) ZnWO₄, (b) ZnWO₄-Ar, (c) ZnWO₄-N₂ and (d) ZnWO₄-O₂.

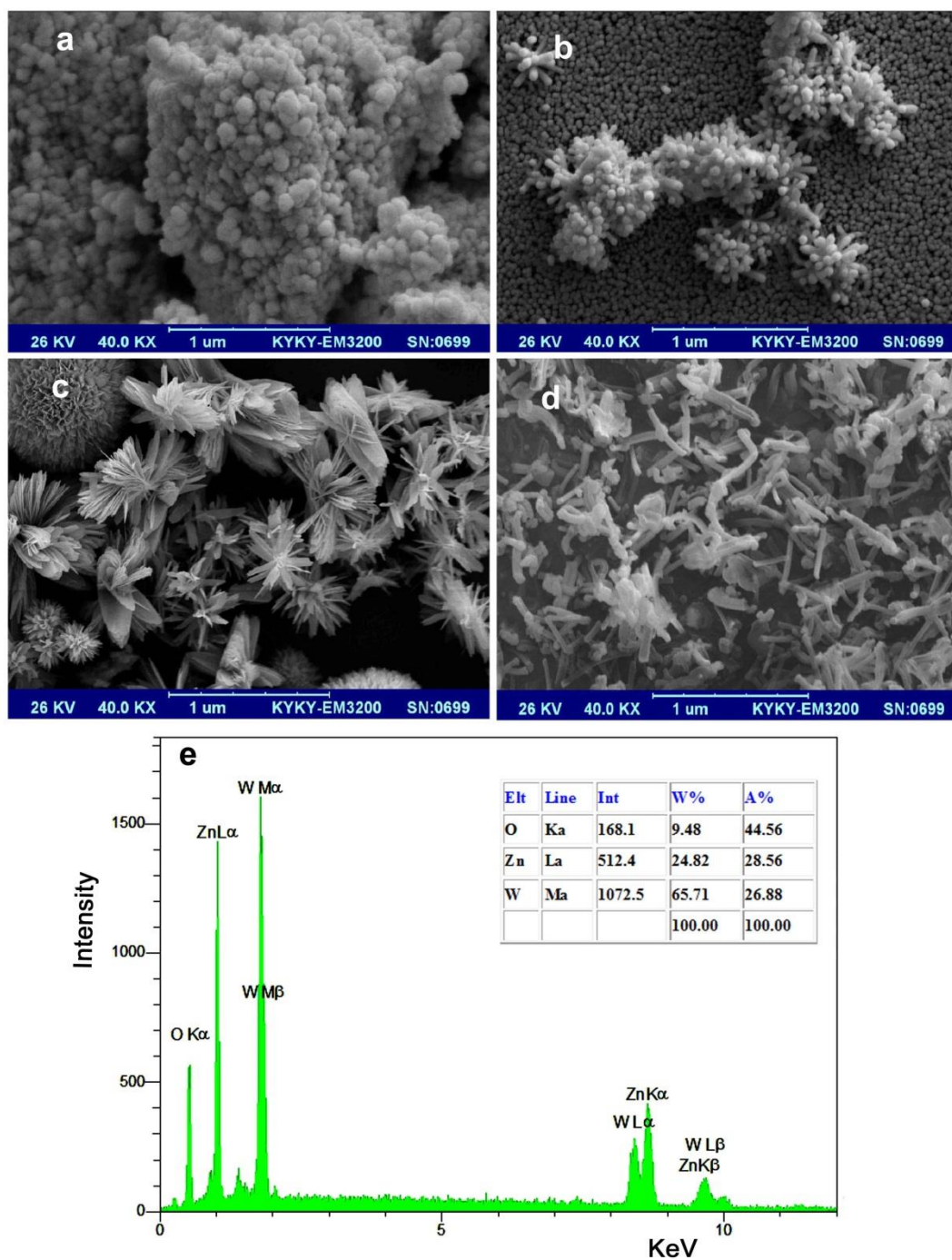


Fig. 3. SEM images of: (a) ZnWO₄, (b) ZnWO₄-Ar, (c) ZnWO₄-N₂, (d) ZnWO₄-O₂ and (e) EDX spectrum of ZnWO₄ nanoparticles.

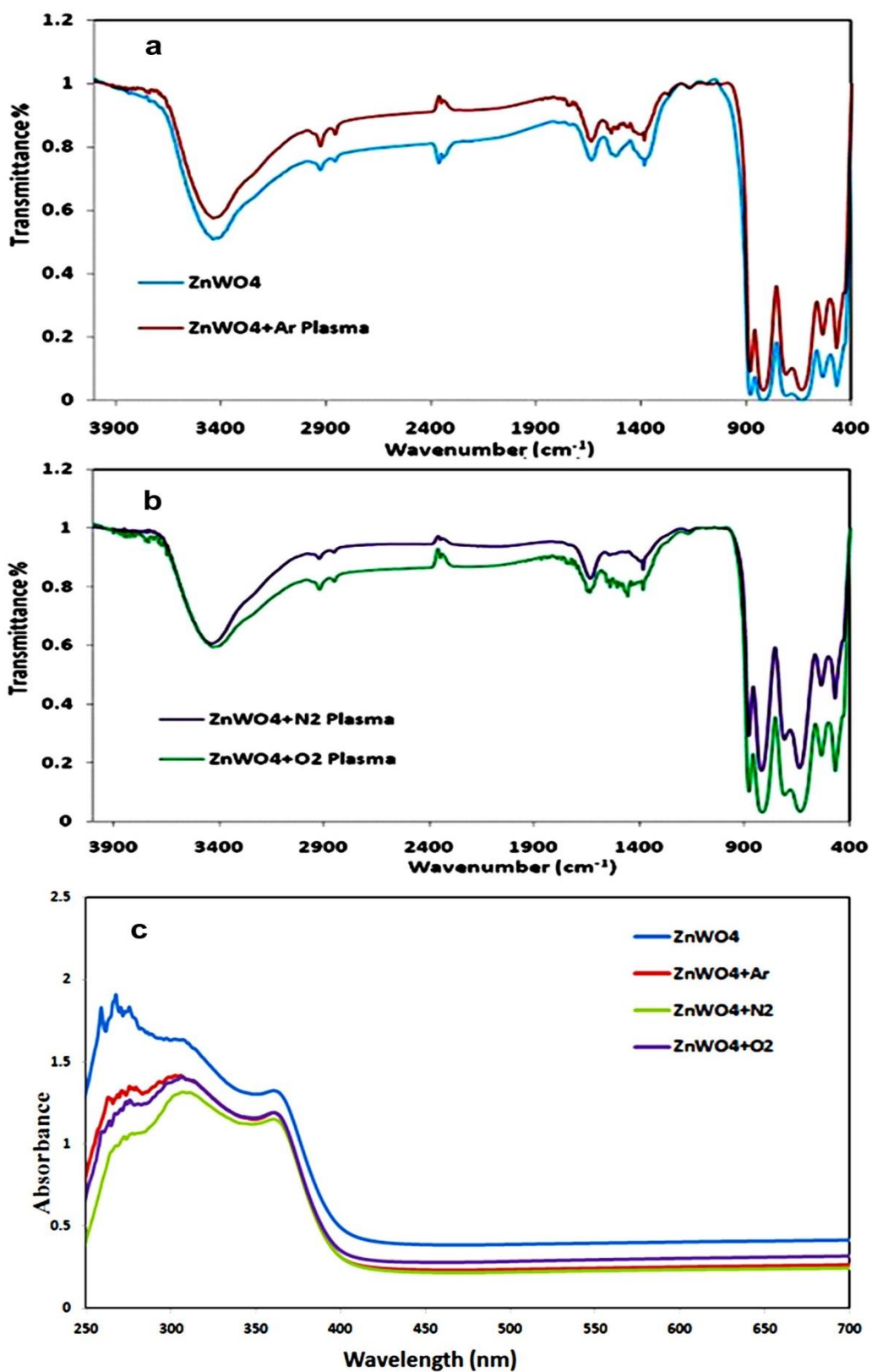


Fig. 4. FT-IR and diffuse reflectance absorption spectrum of ZnWO₄ and plasma-treated ZnWO₄ by different gases

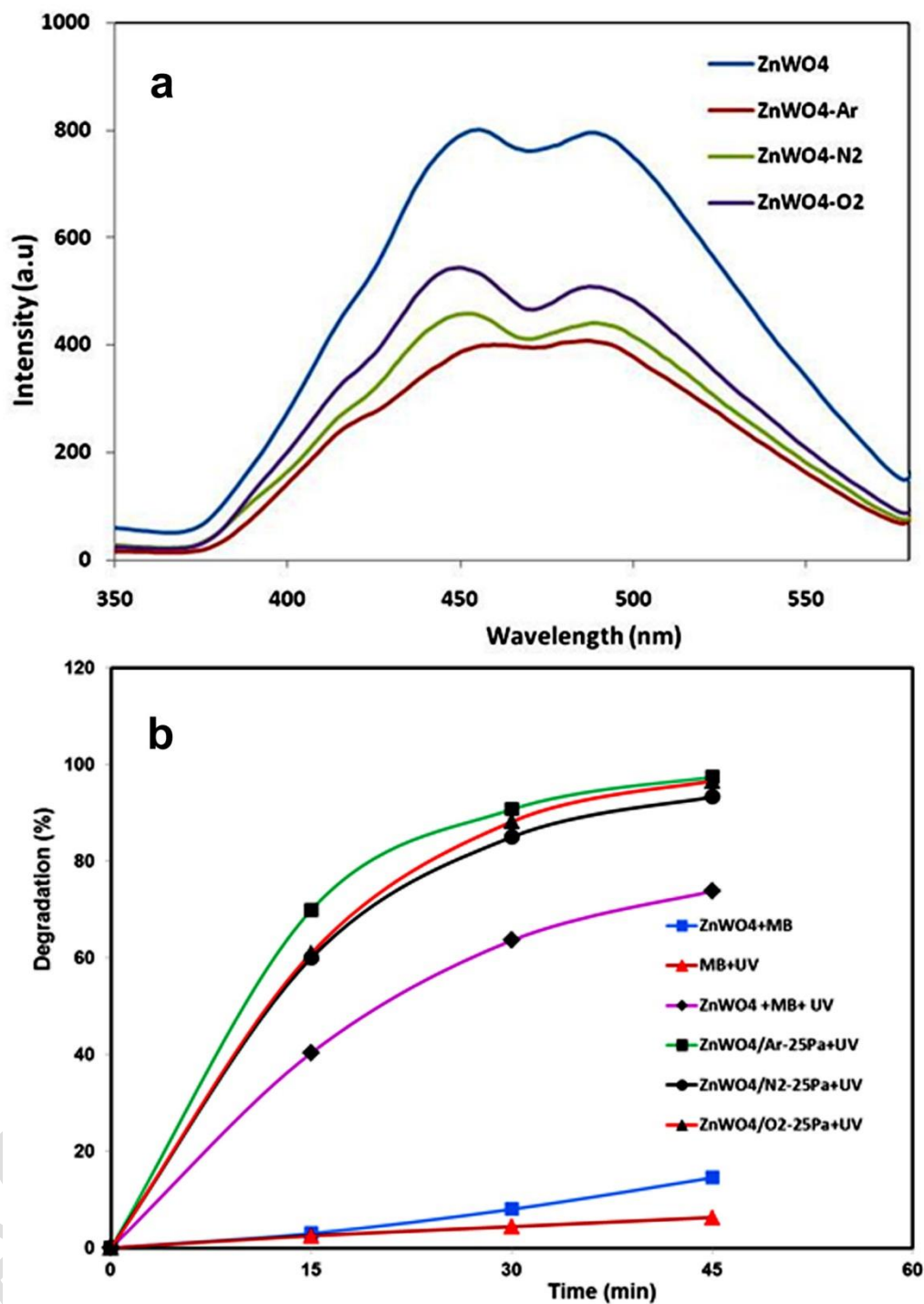


Fig. 5. Fluorescence emission spectra of ZnWO₄ samples with different plasma (a), and (b) Photodegradation of MB in absence and presence of ZnWO₄ and plasma-treated ZnWO₄ at 25Pa under UV irradiation (Experimental conditions: pH = 7, catalyst weights = 40 mg, dye concentration = 1×10^{-5} M and temperature = 25 °C).

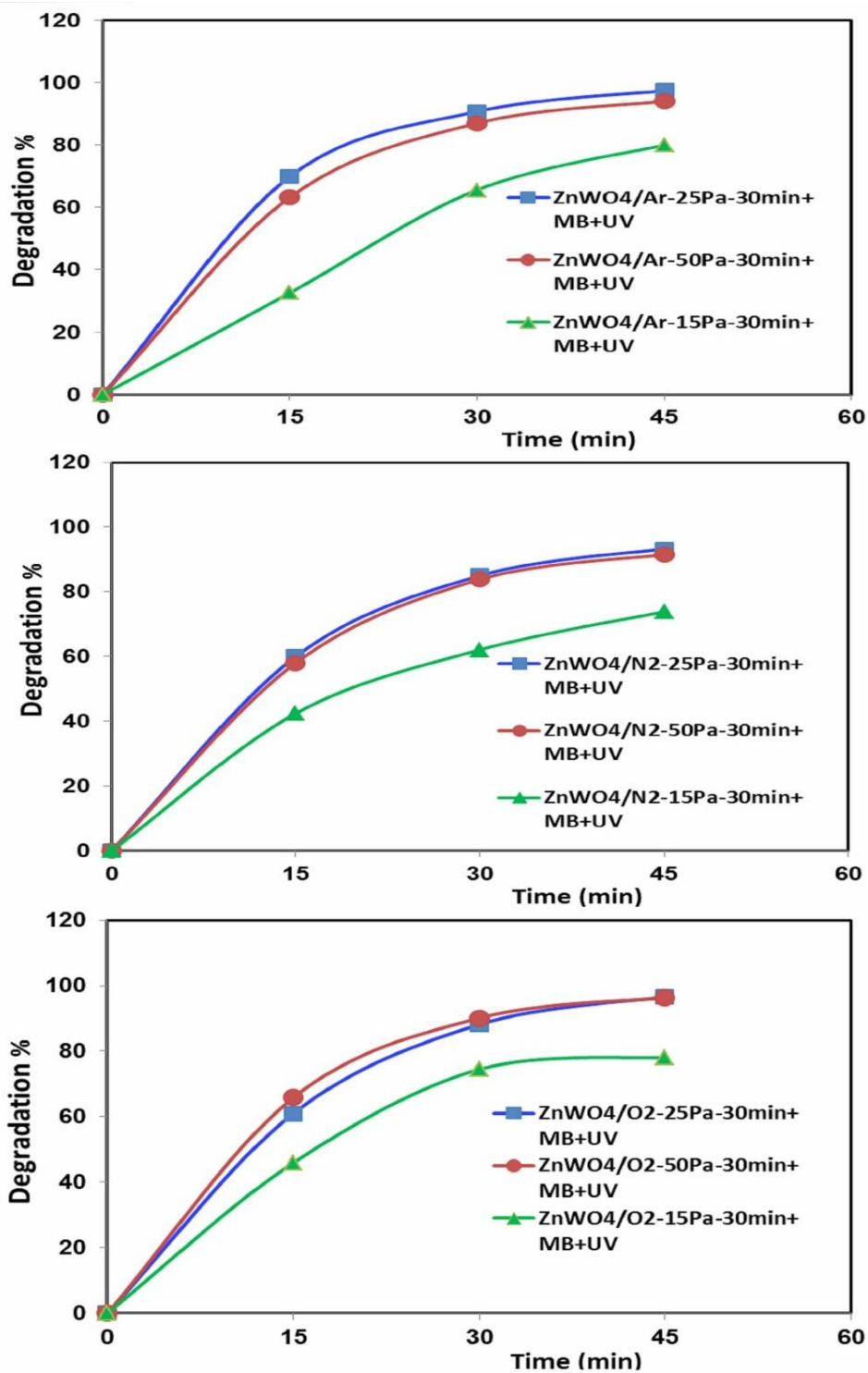


Fig. 6. Photodegradation of MB in presence of treated ZnWO₄ by different gas at different pressure (15Pa, 25Pa and 50Pa) for 30 min under UV irradiation (Experimental conditions: pH = 7, catalyst weights = 40 mg, treatment time = 30min, dye concentration = 1×10^{-5} M and temperature = 25 °C).

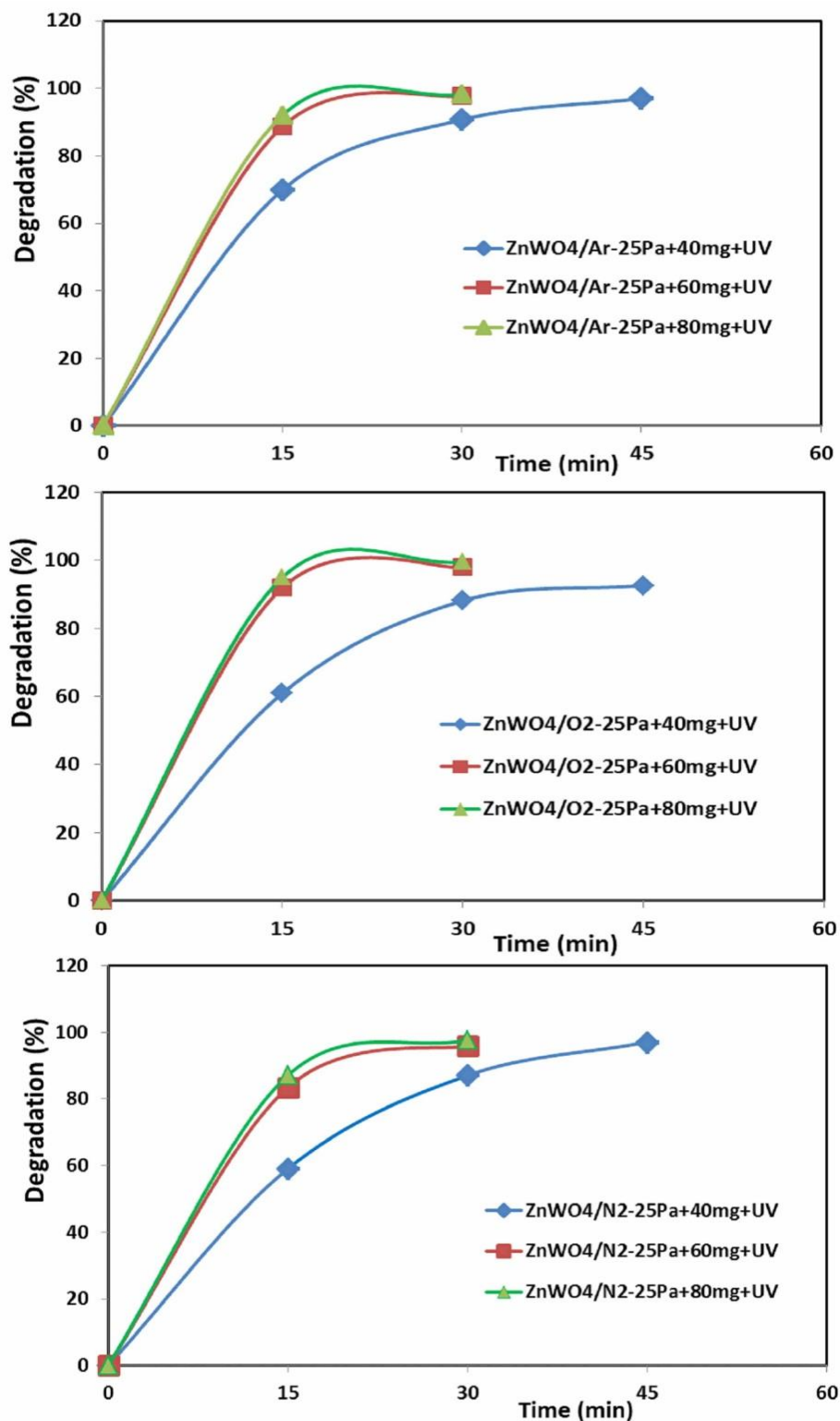


Fig. 7. Photodegradation of MB in presence of different amount of plasma treated ZnWO₄ by different plasma under UV irradiation (Experimental conditions: pH = 7, pressure = 25Pa, treatment time = 30min, dye concentration = 1×10^{-5} M and temperature = 25 °C).

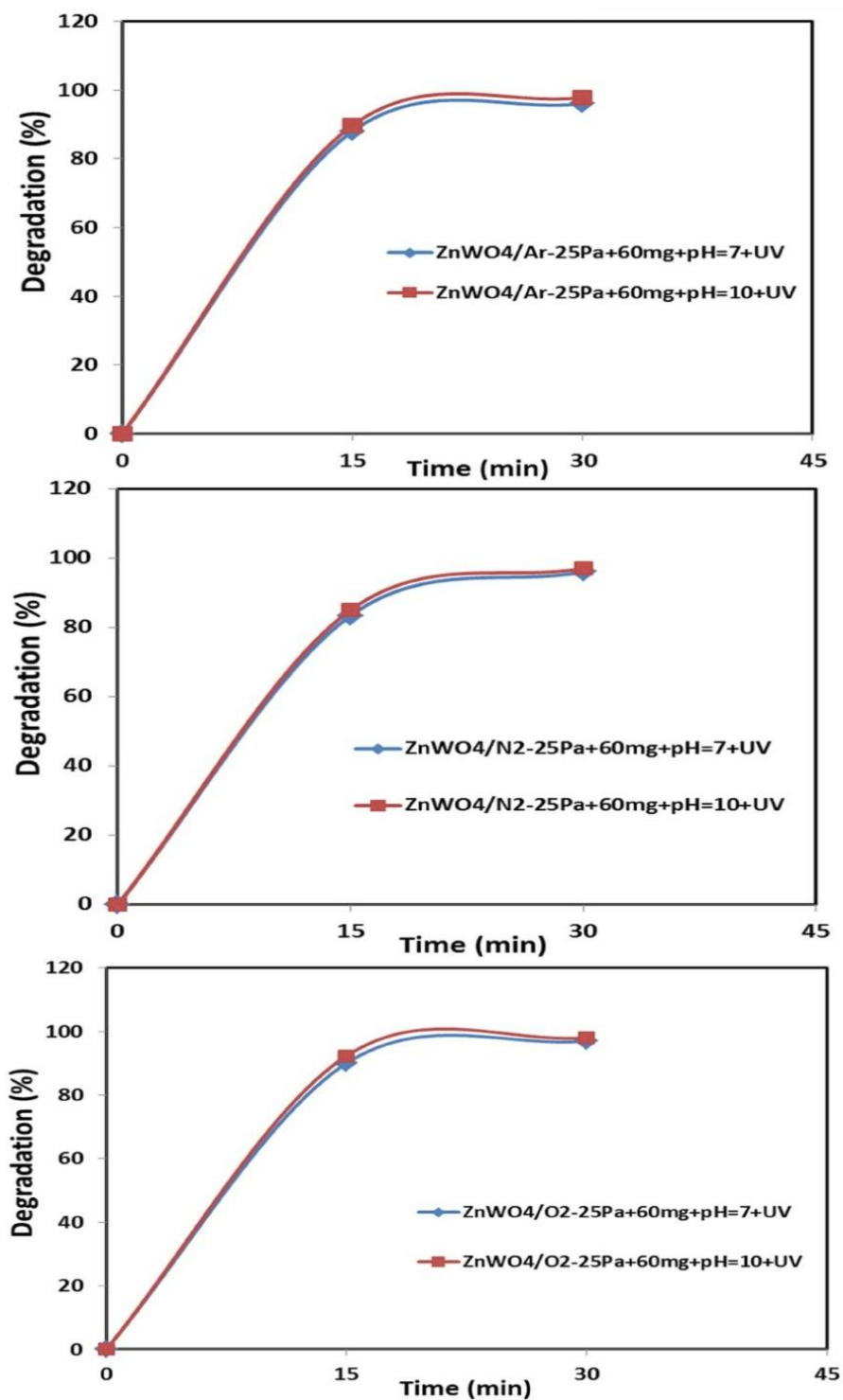


Fig. 8. Effect of pH on the photocatalytic degradation of MB in presence of plasma-treated ZnWO₄ (Experimental conditions: catalyst weights = 60 mg, pressure = 25Pa, treatment time = 30min, dye concentration = 1×10^{-5} M and temperature = 25 °C).

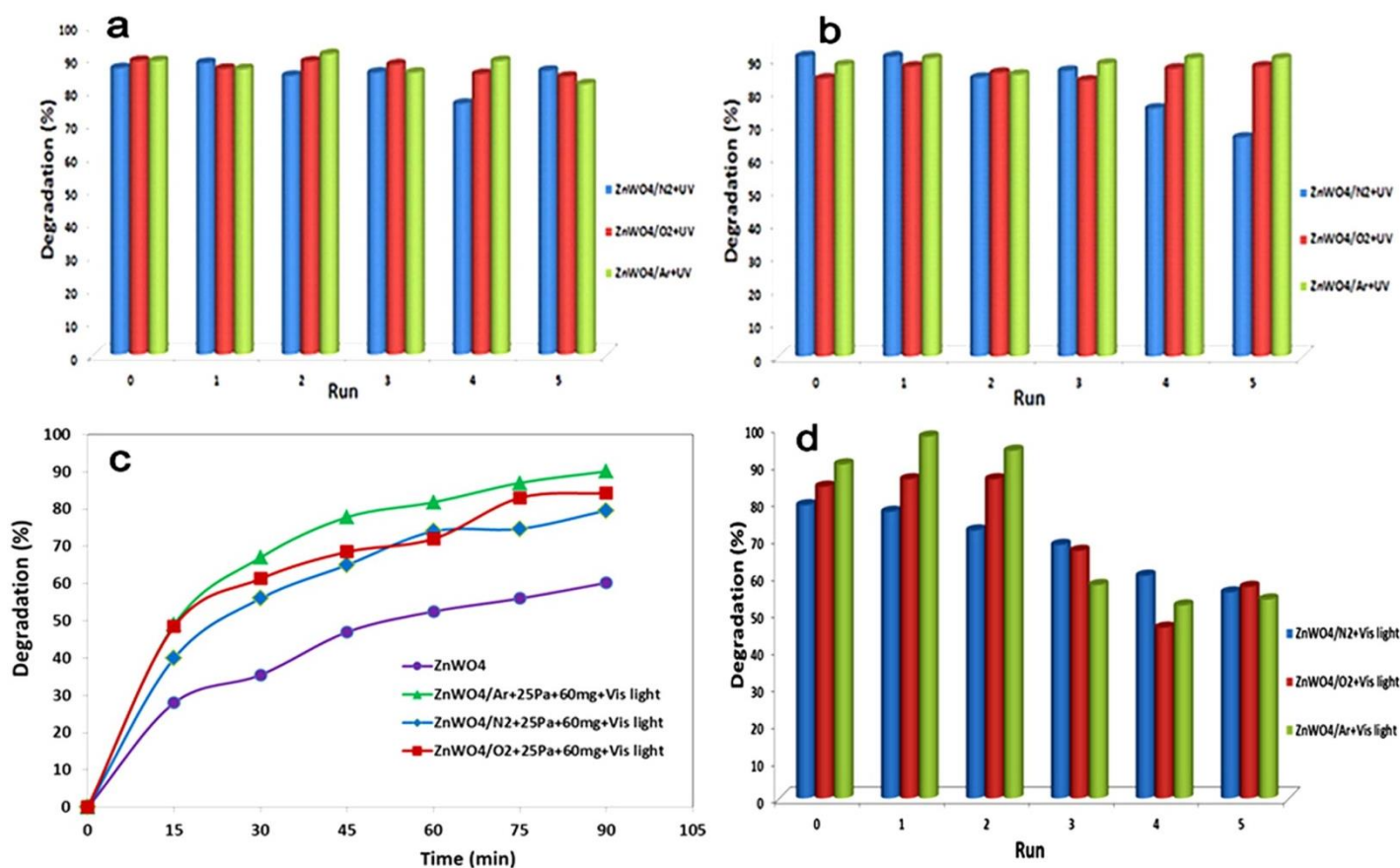


Fig. 9. Cycling runs of plasma treated ZnWO₄ for the photodegradation of MB under UV light at optimized conditions versus number of runs. **(a):** dye concentration = 2×10^{-5} and **(b):** dye concentration 3×10^{-5} M. **(c)** Photodegradation of MB in presence of ZnWO₄ and plasma-treated ZnWO₄ at 25Pa under visible light irradiation (Experimental conditions: pH = 7, catalyst weights = 60 mg, dye concentration = 1×10^{-5} M and temperature = 25 °C), **(d)** cycling runs of plasma treated ZnWO₄ for the photodegradation of MB under visible light at optimized conditions versus number of runs. (Optimized conditions: temperature = 25 °C, catalyst weight = 60 mg, dye concentration = 1×10^{-5} and pH = 7).

Figure captions:

Fig. 1. (a): Schematic diagram of the glow discharge plasma system for treatment of synthesized ZnWO_4 , **(b)** Schematic representation of plasma-treatment on the ZnWO_4 .

Fig. 2: XRD pattern of untreated ZnWO_4 and plasma treated ZnWO_4 : (a) ZnWO_4 , (b) ZnWO_4 -Ar, (c) ZnWO_4 - N_2 and (d) ZnWO_4 - O_2 .

Fig. 3. SEM images of: **(a)** ZnWO_4 , **(b)** ZnWO_4 -Ar, **(c)** ZnWO_4 - N_2 , **(d)** ZnWO_4 - O_2 and **(e)** EDX spectrum of ZnWO_4 nanoparticles.

Fig. 4. FT-IR and diffuse reflectance absorption spectrum of ZnWO_4 and plasma-treated ZnWO_4 by different gases

Fig. 5. Fluorescence emission spectra of ZnWO_4 samples with different plasma **(a)**, and **(b)** Photodegradation of MB in absence and presence of ZnWO_4 and plasma-treated ZnWO_4 at 25Pa under UV irradiation (Experimental conditions: pH = 7, catalyst weights = 40 mg, dye concentration = 1×10^{-5} M and temperature = 25 °C).

Fig. 6. Photodegradation of MB in presence of treated ZnWO_4 by different gas at different pressure (15Pa, 25Pa and 50Pa) for 30 min under UV irradiation (Experimental conditions: pH = 7, catalyst weights = 40 mg, treatment time = 30min, dye concentration = 1×10^{-5} M and temperature = 25 °C).

Fig. 7. Photodegradation of MB in presence of different amount of plasma treated ZnWO_4 by different plasma under UV irradiation (Experimental conditions: pH = 7, pressure = 25Pa, treatment time = 30min, dye concentration = 1×10^{-5} M and temperature = 25 °C).

Fig. 8. Effect of pH on the photocatalytic degradation of MB in presence of plasma-treated ZnWO_4 (Experimental conditions: catalyst weights = 60 mg, pressure = 25Pa, treatment time = 30min, dye concentration = 1×10^{-5} M and temperature = 25 °C).

Fig. 9. Cycling runs of plasma treated ZnWO_4 for the photodegradation of MB under UV light at optimized conditions versus number of runs. **(a):** dye concentration = 2×10^{-5} and **(b):** dye concentration 3×10^{-5} M. **(c)** Photodegradation of MB in presence of ZnWO_4 and plasma-treated ZnWO_4 at 25Pa under visible light irradiation (Experimental conditions: pH = 7, catalyst weights = 60 mg, dye concentration = 1×10^{-5} M and temperature = 25 °C), **(d)** Cycling runs of plasma treated ZnWO_4 for the photodegradation of MB under Visible light at optimized conditions versus number of runs. (Optimized conditions: temperature = 25 °C, catalyst weight = 60 mg, dye concentration = 1×10^{-5} and pH = 7).